Ionization of highly excited helium atoms in an electric field

Willem van de Water,* David R. Mariani,† and Peter M. Koch‡

Josiah Willard Gibbs Laboratory, Yale University, New Haven, Connecticut 06520
and Physics Department, State University of New York at Stony Brook, Stony Brook, New York 11794
(Received 23 December 1983)

We present detailed measurements of ionization of highly excited triplet helium atoms in a static electric field. The atoms were prepared in states with energy E close to the saddle-point threshold $E = -2[F(\text{a.u.})]^{1/2}$. The electric field F was sufficiently strong for the states to be characterized by total spin S and absolute value of the magnetic quantum number M_L. For $M_L = 0$ states the experiments measured ionization properties of adiabatic states. In another case, $|M_L| = 2$, they predominantly measured those of diabatic states. In both cases the ionization rate was found to be a highly nonmonotonic function of the field strength. The observations are analyzed in terms of a theory of the helium density of states in an electric field. A companion paper [D. A. Harmin, Phys. Rev. A 30, 2413 (1984)] develops in detail the general theory, which uses quantum defects to parametrize the effect of the core interaction. The agreement between measured and calculated ionization curves is good, indicating that the field ionization of a nonhydrogenic atom can now be understood in a detailed, quantitative, and predictive sense.

I. INTRODUCTION

The decay by ionization of the resonances (Stark states) of hydrogen atoms in an external, static electric field F is now rather well understood. In the nonrelativistic limit, the Coulomb-Stark potential $V(\vec{r}) = -1/r + Fz$ allows a separation of the Schrödinger equation in parabolic coordinates. When $F \neq 0$, a potential barrier appears in one of the separated equations (usually called the η equation). The decay of the atom in the electric field is associated with the wave-mechanical propagation of the electron either through or over the barrier. In this paper we ignore spontaneous radiative decay. For highly excited atoms the spontaneous decay rate decreases at least as fast as n^{-3} and is negligible compared to field-ionization decay rates of interest in the present paper.[1]

In a given n manifold states whose energies decrease with increasing field strength start broadening at lower field strengths than those whose energies increase with increasing F. For example, the parabolic state $(n_1, n_2, |m|)$, where $n = n_1 + n_2 + |m| + 1$, with the smallest value of n_1 $(0, n-1, 0)$ has the lowest tunneling ionization threshold field, approximately given by $n^4 F \sim 0.1$ a.u.,[2] whereas that with the largest value of n_1 $(n-1, 0, 0)$ has a threshold about a factor of 3 larger, $n^4 F \sim 0.3$ a.u.[2] Ionization rates of some parabolic substates of hydrogen atoms in the $n = 30$ and 40 manifolds that were previously measured by two of us[2] show this behavior and are in good agreement with nonrelativistic, numerical calculations.[3]

Because it is a prototypal resonance problem, the Stark effect in hydrogen has been treated by many different theoretical methods,[4,5] including perturbation techniques,[5,6] numerical integration of the wave equation,[3,5,7] and a modified Jeffreys-Wentzel-Kramers-Brillouin (JWKB) method.[8] The latter is particularly attractive because of its almost analytic character.

Because of the finite extent of the core, the response of a nonhydrogenic atom to an electric field is qualitatively different.[9] The non-Coulombic core potential mixes different parabolic channels, causing anticrossings between levels. The ionization rate (width) of a narrow level can be greatly increased if it is mixed with one or more rapidly ionizing levels that lie nearby in energy. A principal aim of this paper is to characterize these interactions among narrow and broad levels and to examine their role in the ionization process.

Such a channel-mixing phenomenon may also occur[10] in the hydrogen atom. Here the deviation from the pure Coulomb-Stark potential is caused by relativistic (fine-structure) interactions. The predicted magnitude[10] of this effect in hydrogen, however, is much smaller than that produced by the much stronger electrostatic and magnetic interactions in multielectron atoms. For photoexcitation in an electric field of a tightly bound electron to a state whose energy lies near or above the top of the η barrier, the core-induced coupling between narrow and broad parabolic channels can give rise to Beutler-Fano profiles in the cross section.[11] Harmin recently presented a theory[12] for the nonhydrogenic Stark effect which is based on a natural separation of physical space into an inner region, where the interaction of the (Rydberg) electron with the electric field is negligible compared to that with the core, and an outer region where the opposite situation holds. The influence of the core is parametrized by quantum defects, whereas the applied field is always incorporated into parameters of the hydrogenic Stark effect.[8]

When a nonhydrogenic atom is excited in a small electric field that is subsequently increased to values where the atom ionizes, anticrossings may be traversed adiabatically, diabatically, or in a (an) (unknown) mixture of these, depending on the rate of change of the field. Implicit in this terminology are the different time scales of the fast orbital motion of the electron and the slow variation

of the field. Much as in molecular physics, this allows one to contrast adiabatic motion along (Stark) potential curves, where the rapid electronic motion adjusts adiabatically to the changing field, with diabatic transitions between Stark levels that are induced by a dynamic coupling. When anticrossings are traversed adiabatically, the ionization threshold field is approximately given by[13,14]

$$\epsilon = -2(F_{SP})^{1/2} , \qquad (1.1)$$

where ϵ is the energy of the electron at zero field and F_{SP} is the so-called saddle-point field strength, both in a.u.

Because of its importance as a detection technique for highly excited atoms, field ionization has been given much attention. In one experiment with $n \simeq 14$, $|M_L| = 2$ Na atoms, Littman et al.[15] observed and explained a rapid increase of the ionization rate of a narrow state near a relatively isolated anticrossing with a broad level. The theoretical interpretation was keyed to a two-level analysis of the isolated anticrossing. Another experiment[16] observed at the saddle-point threshold a rapid increase of field-ionization signals for adiabatic levels, but actual field dependences of ionization rates were not measured. The challenge of predicting these rates near threshold has been well appreciated (Ref. 9, p. 101). In neither of these experiments were dynamic effects important, which simplified their interpretation.

Many experiments have dealt with situations where dynamic effects are also important.[17] In principle, the response at one or more isolated anticrossings of the atom to the time-varying field may be described by the Landau-Zener-Stückelberg[18,19] formula. In experiments where many closely spaced anticrossings are traversed rapidly, quantitative comparison with theory is as yet an unattained goal. This follows from theoretical difficulties in describing both the atomic structure in the intense field as well as complicated dynamical effects involving many levels.[18]

In this paper we describe an experimental study of the detailed ionization behavior of highly excited helium atoms in an electric field. The atoms were prepared in uniquely defined, adiabatic Stark states close to the saddle-point threshold by a fast-beam, laser-double-resonance method. This technique employed two fixed-frequency infrared lasers which irradiated a fast beam of collisionally excited, triplet ^{4}He atoms as they traversed two spatially separated regions of static electric field. Adjustment of each field strength tuned a certain helium, Stark energy-level splitting into resonance with each laser. Atoms prepared in this way then passed through a region of strong, transverse static electric field. Only those atoms which were not ionized by this field were subsequently detected by field ionization in a longitudinal field. The details of the production and detection of experimental signals are presented in Sec. II.

By carefully controlling the rate of change of the field that the atoms experienced in their rest frames, from the excitation region through the region where ionization took place, we concentrated on the structural aspects of the interaction between atom and field. In Sec. III we present ionization curves recorded in two different kinds of ionization experiments: The first focuses on ionization of diabatic ($|M_L| = 2$) states, the second on the ionization of adiabatic ($M_L = 0$) states. In Sec. IV we explain quantitatively our experimental findings in terms of an analysis of the helium density of states that is based on an adaptation of Harmin's theory[12] of the nonhydrogenic Stark effect. Here it is directed toward a description of relatively narrow (quasidiscrete) Stark levels. (Some details of our theoretical analysis are given in the Appendix. A detailed description of the theory by Harmin[20] appears in an article elsewhere in the same issue of this journal.) It will be shown that field ionization of nonhydrogenic atoms is caused by a core-induced interaction between stable and unstable states. In Sec. V we present our conclusions; we anticipate here the most important one, namely that field ionization can now be understood in a detailed, quantitative, and predictive sense.

II. EXPERIMENTAL METHOD

An important aspect of the experiment is to achieve a well-defined transition from the excitation of a more or less stable state in an electric field to higher-field values where the atom decays more rapidly. By using a fast-beam technique the spatial separation of the field where excitation took place from the field where the decay was studied allowed a precise control over, and reproducibility of, the temporal variation of the field in the rest frame of each atom in the beam. We wish to emphasize the importance of this point. The double-resonance technique used to prepare helium atoms in a single, highly excited triplet state is similar to that recently reviewed by one of us.[21]

A. Apparatus

Figure 1 is a schematic diagram of the apparatus. A fast ($T = 11$ keV), monoenergetic ($\Delta T/T = 3 \times 10^{-3}$) beam of He$^+$ ions collided with Xe atoms contained in a gas cell (not shown in Fig. 1). Electron-transfer collisions produced He $(1s,nl)^{1,3}L_J$ atoms in highly excited states.

The beam then traversed the first region of electric field F_1 where the atoms interacted with photons from a CO_2 laser.[22] By choosing the appropriate values of the laser frequency and the electric field strength, a fraction of the atoms was excited to a well-defined Stark state. The field F_1 ($\simeq 25$ kV/cm) also served to deflect remaining ions from the beam and to ionize atoms with principle quantum numbers $n \gtrsim 10$. A second transition with a separate CO_2 laser was driven in a region of electric field F_3. The intermediate field F_2 avoided a region of zero field between F_1 and F_3. The field strength in F_2 was typically around 200 V/cm. This ensured that the laser-excited state produced in F_1 joined adiabatically at a much lower field strength in F_3 ($\simeq 2$ kV/cm) to a state with the same absolute value of the azimuthal quantum number M_L. Obviously, a necessary condition was that the Stark shift of the levels in the intermediate field be much larger than their fine-structure splitting.[23]

In general, we chose the field strength in F_3 to be close to the saddle-point ionization threshold field F_{SP} for the Stark state chosen for study. The highly excited ($n \simeq 18$) atoms prepared in this state then traversed an intermedi-
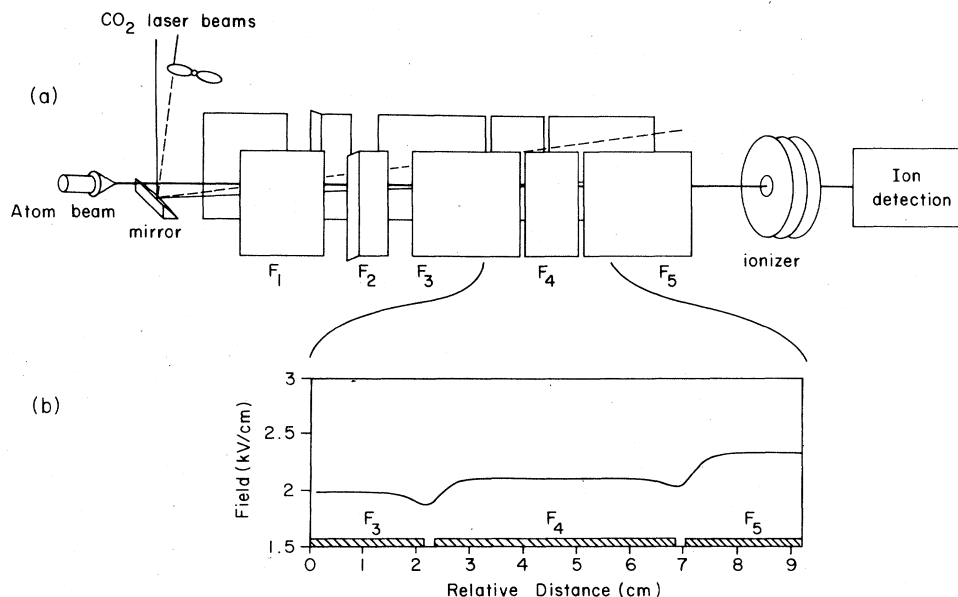
FIG. 1. (a) Schematic drawing of the apparatus. A beam of excited and ground-state atoms enters from the left and is crossed at shallow angles by two different CO_2-laser beams in regions of electric field F_1 and F_3. F_2 avoids a region of zero field between F_1 and F_3. The highly excited atoms emerging from F_3 pass through an intermediate field F_4 into F_5, where they may be ionized. The highly excited atoms which survive passage through F_5 are ionized in a strong longitudinal electric field, and the ions are deflected off axis (not shown) and detected by a Johnston particle multiplier. The output-signal current is detected in phase with the mechanically chopped F_1 laser beam. (b) Calculated transverse electric field on the beam axis as a function of distance in the transition regions F_3-F_4 and F_4-F_5. Only parts of the F_3 and F_5 plates are shown. Their lengths are 8.27 and 8.24 cm, and their separations are 0.9396(5) and 0.9383(4) cm, respectively.

ate field F_4 (also set just below F_{SP}) to enter a field F_5 where their decay was studied. All highly excited atoms which survived passage through F_5 were subsequently ionized in a strong, longitudinal, "detection" electric field F_{det}. It was empirically set to saturate the detected signal. Because F_5 was transverse to the beam direction, ions produced by field ionization were deflected out of the beam and were lost to the later detection process. Even if ionization took place at the end of the F_5 plates, these ions were deflected by another weak, transverse field (not shown in Fig. 1) located between the F_5 plates and the longitudinal "detection" field.

The emerging signal ions were deflected into a Johnston particle multiplier which was operated as a linear current amplifier. A lock-in amplifier measured the multiplier's output signal in phase with a modulation which mechanically chopped the laser beam interacting in F_1. The output signal from the lock-in amplifier was digitized in a voltage-to-frequency converter and stored in a multichannel analyzer operated in the multiscaling mode. The voltage on the plates F_5 was varied synchronously with the analyzer's channel address, thereby permitting an automated measurement of the number of atoms which survived passage through F_5 as a function of the field strength in F_5. By taking a large number of sweeps, slow variations in particle and laser-beam intensities were averaged out. The repetitive sweeping of the voltage on the plates F_5 was sufficiently slow $[O(10^{-1}$ Hz)] that the resultant rate of change of the field was negligible compared to that experienced by the atoms moving swiftly from one region of electric field to another.

To ensure smooth transitions between the differing field strengths in regions F_3, F_4, and F_5, the distance between adjacent pairs of field plates was made as small as possible. (See Ref. 24 for construction details.) Figure 1(b) shows, for a typical experimental situation, the calculated fields on the atomic-beam axis in the F_3-F_4 and F_4-F_5 transition regions. The maximal rate of change of the fields in the rest frame of atoms traveling at a beam energy of 11 keV there was approximately 4×10^{10} V/cm s.

The separations between opposing pairs of F_3, F_4, and F_5 field plates were measured mechanically and compared with those obtained from an analysis of Stark-tuned, laser-driven transitions between known initial and final hydrogen parabolic states (belonging, respectively, to the $n = 10$ and $n = 36-39$ manifolds).[25] For this purpose an atomic hydrogen beam was used in place of a helium beam; the apparatus was otherwise identical. For the field strengths ($F \sim 10^2$ V/cm) and n manifolds used, the energies of the states could be approximated by Rayleigh-Schrödinger perturbation theory evaluated up through eighth order.[6] Knowing the laser wavelength and the hydrogen-beam velocity, which caused a Doppler shift, the field required to tune the desired atomic energy splitting into resonance with the laser photons could be calculated. The separation of the plates then followed from the accurately measured voltage difference applied to the plates. By comparing the voltage positions of Stark-tuned hydrogen transitions for both polarities of the applied potential difference, the possible influence of surface charge effects and motional electric fields[24] could be ascertained. For all our electric field plates those effects were observed
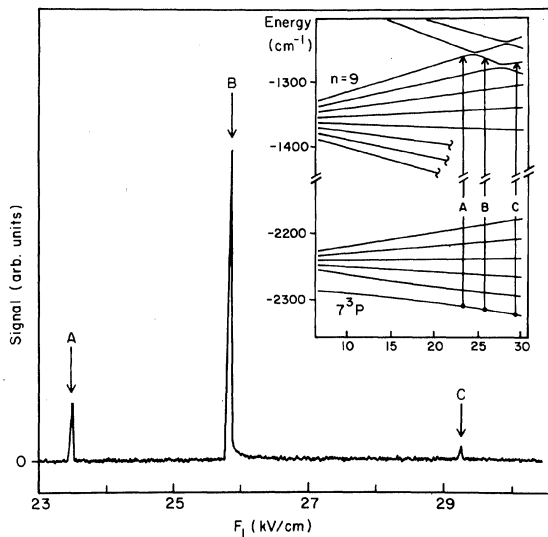
FIG. 2. Signal of triplet He atoms excited in F_1 with a fixed laser frequency from the adiabatic "7^3P" ($M_L=0$) state to the adiabatic "$9^3(L=8)$" ($M_L=0$) state as a function of the field strength. The inset shows the relevant part of a Stark map of the $M_L=0$ manifold that was calculated by matrix diagonalization. The arrows A, B, and C indicate where the calculation predicted that transitions would occur. The occurrence of these three Stark-tuned resonances is shown schematically in the inset. The "$9^3(L=8)$" atoms were detected via CO_2-laser excitation in the F_3 region to a higher-lying Rydberg state which was detected by field ionization (see Fig. 1 and the text).

to be negligible. The mechanical and spectroscopically derived measurements of the separation of each electrode pair agreed to within 0.3%. We adopted this 0.3% discrepancy as a conservative estimate of the error. The line shape of the peaks in a helium Stark spectrum such as that shown in Fig. 2 is asymmetric. The tail on the high-field side is mainly caused by the fringe fields of the plates. The much smaller tail on the low-field side reflects the field inhomogeneity. For the set of plates indicated as F_5 in Fig. 1 this was estimated to be $\Delta F/F = 5.2 \times 10^{-4}$.

By varying the strength of the intermediate field F_4, the rate of change of the field experienced by atoms going from F_3 into F_4 and from F_4 into F_5 could be changed. This provided a direct experimental test for evaluating the importance of transitions at avoided crossings between different adiabatic energy levels.

B. Spectroscopy

The principal aim of the laser double-resonance excitation scheme was to produce a beam of atoms in uniquely defined Stark states, as characterized by the electric field strength, their energy position, and the values of the S and the $|M_L|$ quantum numbers. We assumed that, for the present range of field strengths, to a good approximation, the He states were eigenstates of the component L_z of the orbital angular momentum operator in the field

direction and of the total spin angular momentum operator S.

Upon entering the first region of electric field F_1, the atoms were in a distribution of He $(1s,nl)^{2S+1}L_J$ states, where the n distribution (summed over L and M_L) is close to n^{-3}.[21] The CO_2 laser operated on fixed frequencies from a spectrum of about 50 lines in the P and R branches of two bands near 10^3 cm^{-1}. Transitions in an electric field were driven by choosing an appropriate laser line and Stark-shifting the levels until the (Doppler-shifted) photon energy matched the energy difference between two levels at a particular value of the field strength. Apart from determining their energy positions, the electric field also influenced the electric dipole matrix elements between the corresponding states. Taking the latter fact into account was of utmost importance in devising an efficient excitation scheme.

Figure 2 illustrates the first step of a two-laser, double-resonance excitation scheme:

$$\text{"}7^3P\text{"} \ (M_L=0) \rightarrow \text{"}9^3(L=8)\text{"} \ (M_L=0)$$

$$\rightarrow \text{"}n=19^3L\text{"} \ (|M_L|=1) \ ,$$
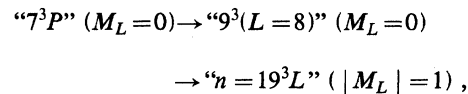
where the quotation marks enclose the zero-field state to which the Stark state joins adiabatically when $F \rightarrow 0$. The 9-μm $P(16)$ laser line was used, and with the laser polarization parallel to the electric field direction, the selection rule $\Delta |M_L| = 0$ pertained. As the inset in Fig. 2 shows, the "$9^3(L=8)$" state takes part in anticrossings with other $n=9$ and 10 states. At a fixed photon energy, transitions occurred at several values of the field strength in F_1, but their oscillator strengths were very different. The data show that the strongest transition occurred when the adiabatic "$9^3(L=8)$" state assumed the downward-going character of the "10^3S" state, in accordance with the expectation that transitions between states having dipole moments of the same sign are (grossly) favored over those between states having dipole moments of opposite sign.

The energy levels were calculated using a matrix-diagonalization technique described by Zimmerman et al.[26] The wave functions were expanded using a set of 81 spherical basis states from the $n=5-13$ manifolds. To calculate the interaction matrix elements it was assumed that the valence electron moved in a pure Coulomb potential. The only allowance for electrostatic fine-structure and exchange effects was made through the triplet helium quantum defects, which we obtained from Seaton.[27] As is well known, the procedure for calculating the dipole interaction matrix elements for nonhydrogenic atoms using only Coulomb wave functions and quantum defects was introduced by Bates and Damgaard.[28]

The arrows labeled A, B, and C in Fig. 2 show our calculated values of the field strength in F_1 where the respective transitions shown in the inset should occur. The agreement between the calculated and measured F_1 values is within the width of the peaks. When, after being excited to the "$9^3(L=8)$" state, the atoms left the first region of electric field F_1 and entered the much lower value of the field strength in F_2, the anticrossings shown in Fig. 2 were traversed adiabatically. The field plates F_2 (Ref. 24) between F_1 and F_3 provided a field (typically around

200 V/cm) which was sufficiently large for the state to remain defined uniquely.

In a third region of electric field F_3 the atomic beam interacted with a beam of photons from a second CO_2 laser which induced transitions to $n \sim 18$ states whose $|M_L|$ value depended on the orientation of its plane of polarization. The excitation occurred at a field strength which was set to be close to the saddle-point ionization limit [Eq. (1.1)]. At these values of the field strength the $M_L = 0, n \sim 18$ parabolic channels (i.e., the hydrogenic states) were strongly mixed. A plot of $M_L = 0$ energy levels (see Fig. 3) shows large anticrossings and almost no resemblance to a plot of the corresponding hydrogenic levels. However, the same general trend mentioned above applies to the magnitude of the transition matrix elements. Since the intermediate state was one with an extreme dipole moment (it was the most upward-going state of the $n = 9$ manifold), we expected that transition matrix elements would be large for those values of the electric field where an adiabatic state assumed the character of the hydrogenic $n = 18$ state with the largest dipole moment.

That this was indeed the case is shown in Fig. 3. For a fixed laser line the number of laser-excited atoms emerging from F_3 is plotted as a function of the field strength F_3.[29] The laser was tuned to the 9-μm P(20) line and was linearly polarized parallel to the electric field direction. The inset of Fig. 3 shows energy levels for $M_L = 0$ calculated by matrix diagonalization. The dashed line indicates the "$9^3(L = 8)$" state displaced upwards by an energy $h\nu'$, where ν' is the Doppler-shifted laser frequency in the rest frame of the fast atoms. A transition could occur at every crossing of this line with an adiabatic potential curve. The data show that at the crossing labeled γ, the transition signal was much larger than at those labeled α and β. No signal was observed for the unlabeled crossing between β and γ. A closer analysis reveals that a large transition matrix element, and consequently a strong signal, occurred at those field values where an adiabatic helium energy level was approximately tangential to the energy of the $(n_1, n_2, |M_L|) = (17,0,0)$ hydrogen state. This circumstance was crucial for our experiment. By choosing different laser lines we were able efficiently to prepare a beam of atoms in different, uniquely defined Stark states close to the saddle-point ionization limit F_{SP}.

From Fig. 3 it is evident that the matrix-diagonalization procedure sufficed to establish which adiabatic state was produced in F_3 ($< F_{SP}$). However, we found that it did not enable us to predict the evolution of the atom when the field was increased beyond F_{SP}. There are two reasons for this, the first involving practical considerations, the second being more fundamental.

(i) To attain numerical convergence of the calculated energy-level positions over a limited energy interval for fields close to F_{SP}, a very large number of basis states has to be included. This number increases rapidly with the field. For the calculations that produced the inset in Fig. 3, 216 basis states belonging to the $n = 17 - 26$ manifolds were used.

(ii) Many of the Stark-shifted states belonging to the higher manifolds in the perturbation expansion are significantly broadened at about 2 kV/cm. Since the expansion
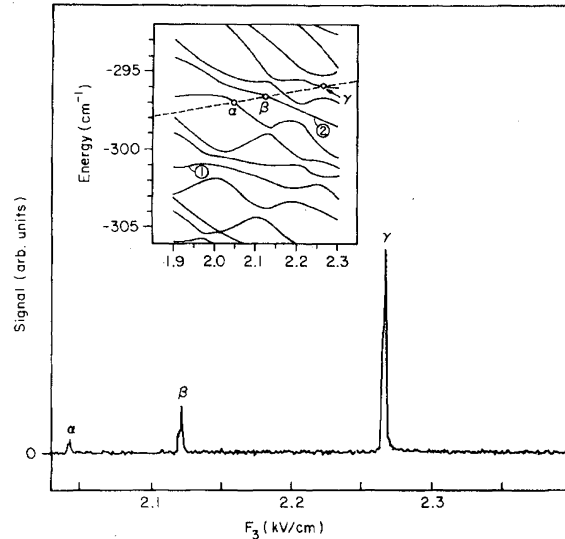

FIG. 3. Signal of triplet He atoms excited in F_3 from the "$9^3(L = 8)$" ($M_L = 0$) state to states lying close to the saddle-point ionization threshold (e.g., $F_{SP} = 2.32$ kV/cm at $E = -295$ cm^{-1}). The inset shows the relevant part of a Stark map of the $M_L = 0$ manifold that was calculated by matrix diagonalization. The dashed line indicates the initial "$9^3(L = 8)$" ($M_L = 0$) state displaced upwards by the Doppler-shifted photon energy of the F_3 laser. The points labeled α, β, and γ locate the Stark-tuned, laser-driven transitions from the "$9^3(L = 8)$" ($M_L = 0$) state at crossings of the dashed line and the upper Stark states shown in the inset. The circled numbers indicate different adiabatic states to which reference is made in the text.

basis only includes discrete states, no allowance for the continuum nature of Stark states is possible.

In Sec. IV we show how a different calculational method based upon a theory involving the helium density of states[12] was used to solve both problems (i) and (ii).

III. EXPERIMENTAL RESULTS

A. Ionization of $M_L = 0$ states

Because of the large core penetration of the triplet s-electron wave function, the level separation at nearly all anticrossings in the $M_L = 0$ manifold of triplet helium levels in an electric field is large (between 0.1 and 1 cm^{-1} for $n \sim 18$). The strength of the core interaction is gauged by the triplet s quantum defect, $\mu_0 = 0.297$ for $n = 18$.[27]

For the $M_L = 0$ measurements discussed here, we expect, on the basis of the following calculation, that all anticrossings were traversed adiabatically; consequently, the measurements reflect the ionization behavior of adiabatic states. The probability for transition from one adiabatic state to another at isolated anticrossings may be estimated from the Landau-Zener-Stückelberg formula.[19] The maximal rate of change of the field experienced by atoms which were excited close to the saddle-point ionization limit, and which subsequently traveled through the fringe fields between F_3-F_4 and F_4-F_5, is estimated from Fig.

1(b). It depicts a typical field configuration for the $M_L = 0$ measurements. Using $dF/dt < 4 \times 10^{10}$ V/cm s, a difference in slope of the levels $d(\Delta E)/dF < 4 \times 10^{-2}$ cm^{-1}/(V/cm), and a level separation $\Delta > 0.1$ cm^{-1}, we calculate a transition probability $P < 10^{-1}$. Moreover, our conclusion that the $M_L = 0$ measurements reflected the ionization behavior of adiabatic states was tested by varying the intermediate field F_4 over a range of values which caused the rate of change of the field in the rest frame of the atoms to vary up to a factor of 2. That no change in the ionization curves was observed implies that the transition probability was well below the upper limit calculated above.

Figure 4 shows the ionization behavior of two adiabatic states as a function of the field strength. The numbers in circles indicate the adiabatic states as shown in the inset of Fig. 3. Both states disintegrate at field strengths close to the saddle-point threshold, but the ionization signal (and, therefore, the ionization rate) is a highly nonmonotonic function of the field strength. Especially for the state indicated as (1) the ionization rate shows many oscillations that eventually disappear at considerably higher field strengths than the saddle-point threshold. Because the atoms spent a time $4.67(2) \times 10^9$ a.u. [$1.130(5) \times 10^{-7}$ s] between the plates of F_5, the scatter of the data in the upper and lower asymptotes of the ionization curves in Fig. 4 limits the sensitivity of the experiment to ionization rates in the range $4 \times 10^{-12} < \Gamma < 10^{-9}$ a.u. ($2 \times 10^5 < \Gamma < 4 \times 10^7$ s^{-1}). Rates below (above) this range produce

imperceptible deviations of the ionization curve from the upper (lower) asymptotes.

Because the oscillations observed in the ionization curves are clearly influenced by the quantal structure of the atom in the electric field, a simple classical model of the field-ionization process of nonhydrogenic atoms[13] will be inadequate for an understanding of their origin. The structure that we observe in the ionization rate can, in each case, be unambiguously associated with the response of a single adiabatic state to an electric field. McMillian et al.[30] allude to the occurrence of similar structure in the field ionization of highly excited Na atoms; in their case, however, dynamic effects played an important role.

B. Ionization of $|M_L| = 2$ states

Figure 5 shows a very restricted portion of an ionization curve for a triplet $|M_L| = 2$ state. The points in the figure represent a measured signal proportional to the survival probability for atoms exposed to the electric field F_5 as a function of that field strength. Near $F_5 = 3585$ V/cm a very sharp feature occurs, corresponding to a rapid increase of the ionization rate of the initially populated state. The observed structure is similar to that observed by Littman et al.[15] in the ionization rate of a highly excited sodium $|M_L| = 2$ state. Another localized anomaly in the ionization rate, now of a broad state, was recently reported by Feneuille et al.[31]

Because the core penetration of the triplet d-electron wave function is very small [quantum defect $\mu_2 = 0.0028$ for $n = 18$ (Ref. 27)], the helium triplet $|M_L| = 2$ states in an electric field are almost hydrogenic. Therefore, we shall designate the $|M_L| = 2$ diabatic states by parabolic $(n_1, n_2, |M_L|)$ quantum numbers. The (15,0,2) state con-
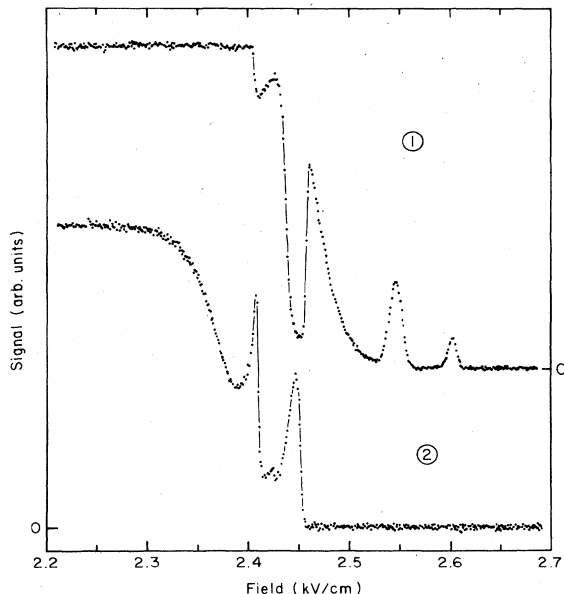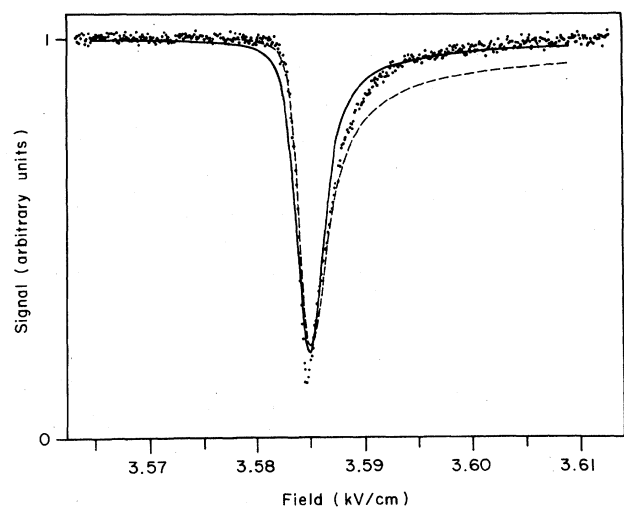

FIG. 4. Signal of highly excited triplet He atoms of the $M_L = 0$ manifold which survived exposure to the electric field F_5 as a function of that field strength (see text for the relevant time scales). The curves show the ionization behavior of two different adiabatic states. They correspond to the states labeled by the same circled numbers as those in the inset of Fig. 2, which shows the energies of these states at smaller field strengths.

FIG. 5. Signal of highly excited triplet He atoms of the $|M_L| = 2$ manifold which survived exposure to the electric field in F_5 as a function of that field strength (see text for the relevant time scales). Points, measured data; solid curve, fit to the data using Eq. (3.3); dashed curve, fit to the data using Eq. (3.5) (see text).

sidered here was populated at $F_3 = 2.768$ kV/cm. Because this is considerably below the range of F_5 values shown in Fig. 5, and because the typical level separation at anticrossings is so small ($\sim 10^{-2}$ cm^{-1}), it is tempting to assume that all anticrossings were traversed diabatically at the rates of change of the field in our experiment. We shall see below, however, that this was not always the case.

At a field strength of 3.581 kV/cm the narrow hydrogenic (15,0,2) state crosses the (7,11,2) state, whose calculated width is 8×10^{-9} a.u. The calculated width of the (15,0,2) state is 10^{-40} a.u. Figure 6 shows the energies of both states as a function of field strength. The energies and widths were calculated using Harmin's modified JWKB method. Within the energy and field intervals of interest there is actually another very diffuse state whose influence can be neglected because of its large width ($\sim 10^{-5}$ a.u.). Owing to the core-induced coupling between the (15,0,2) and (7,11,2) states, the width of the diabatic (15,0,2) state [i.e., the He state which far from the anticrossing corresponds to the hydrogenic (15,0,2) state] is a rapidly varying function of the field strength. Right at the anticrossing, its width, and thus its ionization probability, is maximal and approximately half that of the (7,11,2) state.

In a simplified approach the energies and widths of the helium states near the anticrossing are the real and imaginary parts of the eigenvalues of the energy matrix

$$\left| \begin{array}{cc} E_1 - \dfrac{i\Gamma_1}{2} + \beta_{11} & \beta_{12} \\[2ex] \beta_{21} & E_2 - \dfrac{i\Gamma_2}{2} + \beta_{22} \end{array} \right| , \qquad (3.1)$$

where E_i and Γ_i are the (field-dependent) resonance centers and widths of the hydrogen parabolic channels $|\varphi_i\rangle$, and $\beta_{ij} = \langle \varphi_i | V_c | \varphi_j \rangle$ is the matrix element of the core potential. As has been discussed by Lamb,[32] when

$$4 |\beta_{12}|^2 \le \tfrac{1}{4}(\Gamma_1 - \Gamma_2)^2 , \qquad (3.2)$$

the helium levels cross exactly, in the sense that the real parts of their energies are equal.

Assuming diabatic traversal of the relevant anticrossing, a comparison with the experimental results was made by evaluating the survival probability:

$$S = \exp \left[- \int_l \gamma_1(F(x))dx/v \right] , \qquad (3.3)$$

where $\gamma_1/2$ is the imaginary part of the eigenvalue of Eq. (3.1) which, far from the anticrossing, corresponds to that of the (15,0,2) diabatic state. The function $F(x)$ represents the strength of the electric field on axis, which was almost constant between the plates and fell off rapidly in the fringe-field regions. Those regions were included in the integration interval.

The assumption of purely diabatic traversal of the anticrossing is, however, not justified in our case. This is illustrated suggestively in Fig. 7(a) where $F(x)$, the electric field on axis, is plotted as a function of distance in from the entrance edge of the F_5 plates. Shown is a region inside the plates where the field strength smoothly ap-

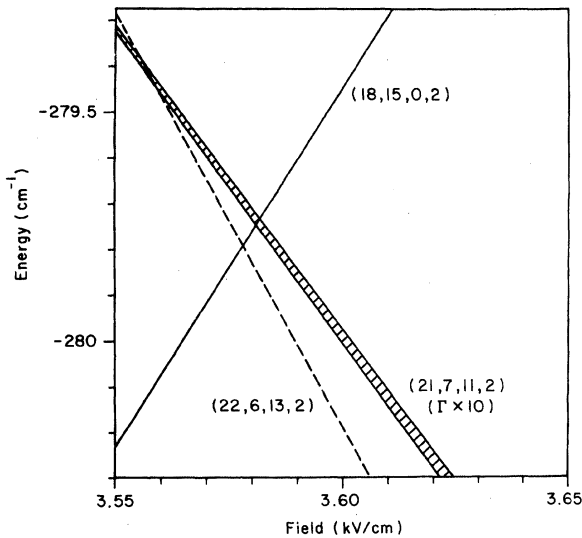FIG. 6. Calculated energies and widths of parabolic hydrogen states of the $|M_L| = 2$ manifold as a function of the field strength. The width of the $(n,n_1,n_2, |M_L|) = (21,7,11,2)$ state is shown multiplied by 10. The dashed line indicates the diffuse (22,6,13,2) state whose width is about 2 cm^{-1}.
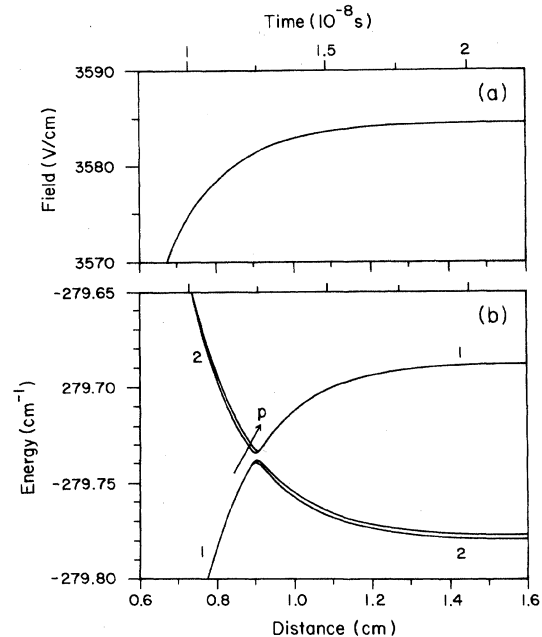

FIG. 7. (a) Calculated strength of the field on axis between the plates F_5 as a function of the distance in from the entrance edge of the plates. The upper horizontal axis shows the time elapsed since the atoms passed the entrance edge of the plates. Notice that the plate edge is off the horizontal axis. (b) Variation of the energies of the $(n,n_1,n_2, |M_L|) = (18,15,0,2)$ and (21,7,11,2) parabolic states with distance (time) for the field shown in (a). The states are coupled through the He$^+$ (1s) core interaction. The transition probability for diabatic passage through the anticrossing (arrow) between adiabatic states is P.

proaches its asymptotic value. The function $F(x)$ was calculated for a parallel-plate capacitor, in which case $F(x)$ is given by a semianalytic expression.[33] Figure 7 shows a case where the asymptotic value of the field strength was taken to be 3584.5 V/cm, slightly above the level crossing, which was calculated to occur at 3581.38 V/cm. The upper horizontal axis gives the time elapsed since the atoms passed the entranced edge of the plates.

Clearly, when the asymptotic value of the field strength approaches (from above) the value of the field where the anticrossing occurs, the rate of change of the field $dF/dt = vdF/dx$ right at the anticrossing decreases. In the present case, when the difference is only a few V/cm, the probability for diabatic traversal may no longer be unity. Because the measured structure is only a few V/cm wide, we conclude that dynamic effects must be partly responsible for its shape.

The variation of the energy levels with distance (time) corresponding to the field in Fig. 7(a) is shown in Fig. 7(b). The atoms in state (15,0,2) entered from the left through the fringe-field region, and after encountering an avoided crossing, the energy levels became almost parallel

as the atoms penetrated deeper into the field region. When the atoms left the plates, the motion through the exist fringe field could be visualized as a traversal through Fig. 7(b) in the opposite direction. This assumes that the relevant part of the fringe field at the exit of the plates F_s is identical to that at its entrance.

In a crude description of the dynamic effects, the survival probability S would be related to the Landau-Zener-Stückelberg transition probability[19] P as

$$S = P^2, \quad P = \exp\left[\frac{-2\pi |\beta_{12}|^2}{[d(\Delta E)/dF](dF/dx)(dx/dt)}\right] \quad (3.4)$$

where we point out that one of the levels being broadened does not alter the expression for the transition probability. This approximation of the survival probability is, however, not justified when the asymptotic field strength between the plates is set close to the anticrossing field and the transition region dx is no longer small.[34,35] We chose a combination of Eqs. (3.3) and (3.4) as a slightly better description of the dynamic effects in the field interval of interest:

$$S = \exp\left[-2\int_{t_0}^{t_1}\gamma_1(F(t))dt\right]\left[(1-P)^2\exp\left[-2\int_{t_1}^{t_h}\gamma_2(F(t))dt\right] + P^2\exp\left[-2\int_{t_1}^{t_h}\gamma_1(F(t))dt\right]\right], \quad (3.5)$$

where t_1 is the instant when the anticrossing is encountered and t_h is the instant when the atoms have traveled half the length of the plates. The lower bound t_0 is taken to be outside the plates, one plate separation away from the edge. When $P = 1$, Eq. (3.5) is identical to Eq. (3.3).

We tried to reproduce the measure ionization curve (Fig. 5, data) with a calculated survival probability given first by Eq. (3.3) (pure diabatic traversal), and second by Eq. (3.5) (mixed adiabatic-diabatic traversal). The interaction matrix element β_{12} was varied in each case until the best fit (judged visually) was obtained with the measured curve. As may be judged from Fig. 5, this procedure enabled us reasonably to reproduce the measured data with $\beta_{12} = 1.9(3) \times 10^{-8}$ a.u. for Eq. (3.3), and with $1.1(2) \times 10^{-8}$ a.u. for Eq. (3.5). The difference between the two fitted values of the interaction matrix element is clearly an indication of the importance of dynamic effects in the fringe field.

In both calculations the diagonal interaction matrix elements were set to zero and the calculated signal was displaced over 4 V/cm, a shift well within the uncertainty in our field calibration. The calculated signal S was also corrected for the field inhomogeneity, which was assumed to be distributed Gaussian. Its width, ΔF, followed from the analysis of separately measured line shapes of laser-induced transitions to narrow states, which gave

$$\Delta F/F = 5.2 \times 10^{-4}.$$

Because it at least attempts to account for mixed adiabatic-diabatic behavior in the fringe fields, we believe that the value of the interaction matrix element obtained using Eq. (3.5) has more validity than the other value.

The discrepancy between the curve calculated with Eq.

(3.5) (dashed curve in Fig. 5) and the measured (dots) is partly due to our incomplete description of the dynamic effects in the fringe fields. This pertains most when the asymptotic value of the field between the plates is close to the crossing field. The assumption that the field was uniform over the beam cross section could also introduce some error. Obviously, a correct treatment of these dynamic effects would require the integration of the time-dependent Schrödinger equation; it would also require a more adequate description of the fringe field. These questions will be addressed in a forthcoming publication.

For their experiments, Littman et al.[15] also used an analysis based on the non-Hermitian energy matrix equation (3.1). The estimated the interaction matrix element from matrix diagonalization. The validity of this analysis will be established in the next section. It will appear that a description based upon the non-Hermitian energy matrix equation (3.1) follows from a theory involving the non-hydrogenic density of states in an electric field. In particular, we shall show that inequality equation (3.2) plays a key role in the derivation. We shall compare the value of β_{12} obtained with Eq. (3.5) with a value calculated from this theory.

IV. INTERPRETATION

A. The helium density of states

The key quantity in the interpretation of our experimental findings is the non-hydrogenic density of states introduced by Harmin,[12]

$$\underline{D}^F = [\underline{\tilde{Q}}(\underline{H}^F)^{-1}\underline{Q} + \sin\underline{\delta}\,\underline{H}^F\sin\underline{\delta}]^{-1}, \quad (4.1)$$

where

$$Q = \cos\underline{\delta} - \underline{h}^F \sin\underline{\delta} \ .$$

Equation (4.1) expresses the spherical matrix elements of the nonhydrogenic matrix $\underline{D}^F$ in terms of the hydrogenic density-of-states matrix $\underline{H}^F$, its dispersive companion $\underline{h}^F$, and the diagonal matrices $\sin\underline{\delta}$ and $\cos\underline{\delta}$ whose elements are $\sin\delta_l$ and $\cos\delta_l$, where $\delta_l = \pi\mu_l$. The dimensionality of the matrices is the number of non-negligible quantum defects μ_l; in helium triplet Rydberg states this is at most three ($l=0,1,2$). In the case of a single ($l=2$) nonzero quantum defect (which accurately describes the He $|M_L| = 2$ case), Eq. (4.1) reduces to a scalar form:

$$D^F = \frac{H^F}{(\cos\delta - h^F\sin\delta)^2 + (H^F)^2\sin^2\delta} \ , \tag{4.2}$$

which can equivalently be written as

$$D^F = (\sin\delta)^{-2}\mathrm{Im}[(\cot\delta - h^F - iH^F)^{-1}] \ . \tag{4.3}$$

For relatively narrow, isolated hydrogen parabolic states (i.e., for energies below the potential barrier in the η parabolic coordinate), the hydrogenic density of states as a function of energy is a sum of Lorentzians, each center of which is a resonance energy and each width of which gives the corresponding decay rate. The concept of a decay rate is justified because a Lorentzian line shape corresponds to a state decaying exponentially in time.[36]

In the case of an isolated hydrogenic resonance contributing to the nonhydrogenic density of states [Eq. (4.1)], it is shown in the Appendix that the nonhydrogenic density of states again takes the shape of a Lorentzian whose width is the same as the hydrogenic width. However, the core interaction shifts the center of the resonance. One may easily verify an important and useful result: The shifted center of narrow resonances follows from the zeros of the first term in the denominator of Eq. (4.2). The hydrogenic density of states, $\underline{H}^F$, vanishes everywhere except near the center of the resonances, where it will be large. Consequently, $\underline{D}^F$ always vanishes except for energies where the first term in the denominator of Eq. (4.2) disappears.

This simple observation can easily be generalized to the case of many interacting narrow hydrogenic channels contributing to the sum in h^F. Again, the nonhydrogenic levels follow from the zeros of Q; these levels will exhibit anticrossings where the hydrogenic levels cross. The generalization of this result to several nonzero quantum defects involves matrix algebra, with the intuitively appealing conclusion that the centers of nonhydrogenic resonances now follow from

$$\det(\underline{Q}) = 0 \ , \tag{4.4}$$

where the dimension of the matrix $\underline{Q}$ is the number of nonzero quantum defects. This conclusion bears close analogy to a similar result from quantum-defect theory.[37]

An analogous, although more complicated expression, for the widths of the nonhydrogenic energy levels is listed in the Appendix. It applies where the nonhydrogenic density of states has a Lorentzian profile. It is these two parameters, characterizing a resonance in terms of the ener-

gy position and width, which are of key importance in the analysis of our experimental results. The energy position designates the adiabatic energy level, and its width gives, in the case of a Lorentzian line shape, its decay rate. The parametrization of the matrix $\underline{D}^F$ by these two quantities determines the damped oscillatory behavior of its Fourier transform, which is the time dependence of the wave function.

For very narrow energy levels, Eq. (4.4) should give the same energy positions of He Stark levels as the matrix-diagonalization method of Zimmerman et al.[26] In Table I we compare the energy eigenvalues near 300 cm^{-1} for some $M_L = 0$ states at $F = 2.3$ kV/cm that were calculated using matrix diagonalization with those calculated from Eq. (4.4). In the latter case only nonzero quantum defects for s and p states were included, and 17 parabolic channels contributed to the hydrogenic $\underline{H}^F$ and $\underline{h}^F$ which were calculated using Harmin's modified JWKB approach. The matrix-diagonalization method used nonzero s, p, and d quantum defects and a (negligible) energy correction due to core polarization for the higher-angular-momentum states. Table I lists eigenvalues for two sets of basis sets, from which the convergence of the diagonalization method can be judged. The table shows that the results of both methods are in excellent agreement. The large number of basis states (242) needed to attain convergence of the matrix-diagonalization method at a field strength of 2.3 kV/cm, and for the energy interval shown, indicates the great calculational economy and power of the new method. Of course, at higher field strengths, where the levels start to broaden significantly, the perturbative matrix-diagonalization approach is inapplicable.

B. Ionization of $M_L = 0$ states

Figure 8(a) shows the energy levels of He $M_L = 0$ states in a region of electric field around the saddle-point threshold field. The levels were calculated using Eq. (4.4) and assuming only nonzero s and p quantum defects. The figure shows a very broad state coming down from above and interacting with other, more narrow states. Its width increases rapidly with increasing electric field, causing the density of states to broaden out to a continuum at field strengths above 2.5 kV/cm. The vertical line segments in

TABLE I. Some energy levels (in cm^{-1}) of helium atoms in the triplet $M_L = 0$ manifold calculated at a field strength of 2.3 kV/cm. (a) Using matrix diagonalization with 216 basis states from the $n = 17$–26 manifolds. (b) Using matrix diagonalization with 243 basis states from the $n = 17$–27 manifolds. (c) Using a density-of-states approach [Eq. (4.4)] with only 17 parabolic channels and nonzero s and p quantum defects of triplet He, $\mu_{l=0} = 0.297$ and $\mu_{l=1} = 0.068$, respectively.

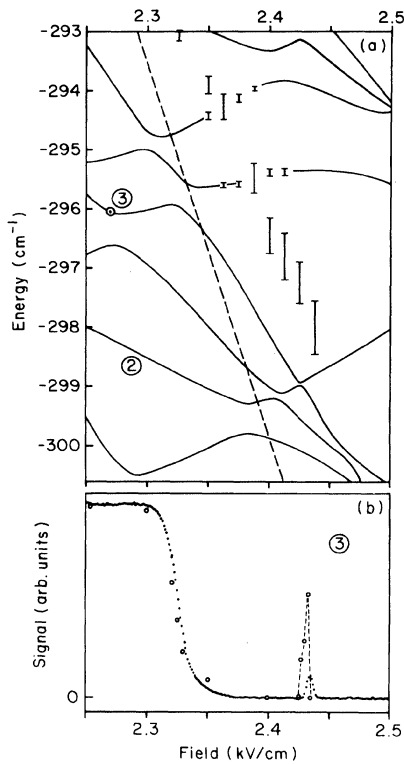| (a)	(b)	(c)
298.528	298.529	298.525
296.946	296.947	296.944
296.040	296.042	296.043
295.020	295.024	295.010
294.714	294.723	294.714

FIG. 8. (a) Calculated Stark map of triplet He levels near the saddle-point threshold $F_{SP} = \epsilon^2/4$ a.u. (indicated by the dashed line). The calculation used the density-of-states formalism. The width of a significantly broadened state is indicated by vertical line segments. The circled numbers label different adiabatic states to which reference is made in the text (see also the inset of Fig. 3). (b) Dots, measured ionization behavior of the adiabatic state which was populated at point 3 shown in the upper part of the figure; open circles, calculated ionization signal.

the figure give an indication of its width (the state is so close to the top of the η barrier that its line shape is no longer Lorentzian). The figure shows that narrow states cross almost exactly with the broad state, in accordance with Eq. (3.2). A careful examination of the density of states at such crossings reveals asymmetric line shapes resembling Beutler-Fano profiles.[38]

Figure 8(b) shows an experimental ionization curve of an $M_L = 0$ adiabatic state. The state was populated at $F_3 = 2.268$ kV/cm, at the point labeled "(3)" in Fig. 8(a). The energy coordinate of this point followed from the calculated energy of the intermediate "$9^3(L = 8)$" state in the double-resonance, laser-excitation scheme, and from the known Doppler-shifted frequency of the laser interacting in F_3. As a test of the calculation we compared the difference between the calculated energies of the intermediate state and the state indicated by "(3)" with the precisely known Doppler-shifted laser frequency. The energies of both states were calculated using Eq. (4.4) and assuming nonzero s, p, and d quantum defects, which depend slightly on the energy.[28] Owing to the 0.3% uncertainty in the calibration of the field strength, the energy difference was calculated to lie in the interval

1049.60(0.05) cm^{-1}. The laser frequency in the rest frame of the atoms was 1049.663(0.005) cm^{-1}. The quoted error in the latter quantity is due predominantly to the velocity spread of the fast atomic beam, and, somewhat less, to the angular spreads in the laser and atomic beams, each of which caused a spread in the Doppler shift (Ref. 21, Sec. 13.4d). The calculated and measured energy difference are in excellent agreement.

The measured ionization curve reveals structure similar to that displayed in Fig. 4. There is a steep decline of the signal near 2.32 kV/cm, followed by a sharp recurrence at 2.43 kV/cm. Comparing Figs. 8(a) and 8(b) one may readily explain the origin of the observed structure. At about 2.3 kV/cm the adiabatic state [indicated by "(3)"] takes on the character of a more rapidly ionizing, downward-going state until it comes to the narrow anticrossing at 2.425 kV/cm. For the range of fields shown, and for the experimental slew rate, this anticrossing was traversed adiabatically. Just to the right of the avoided crossing the adiabatic state takes on the character of a more stable upward-going state, the ionization rate decreases dramatically, and the signal recurs. However, for slightly higher field strengths the state interacts with the very broad descending state and the core-induced mixing causes the ionization rate to increase sharply. Thus it is the interaction with a continuum that forms rapidly in this neighborhood that administers the final "coup de grâce" to the adiabatic state. The core-induced ionization rate remains sufficiently large ($> 10^8$ s^{-1}) to the right of 2.44 kV/cm for the signal never to recur again. The open circles in Fig. 8(b) show a calculated ionization curve at a number of discrete points obtained from the calculated, field-dependent width of the adiabatic state. Since no allowance was made for the fringe field of F_5 in the calculation, the size of the calculated peak is exaggerated. Both the first drop (near 2.32 kV/cm) in the experimental signal and the recurrence at 2.43 kV/cm appear to be at slightly higher field strengths ($\simeq 0.1\%$) than the respective calculated features. This shift, however, is insignificant compared to the 0.3% uncertainty in the experimental field calibration.

C. Ionization of $|M_L| = 2$ states

For triplet $|M_L| = 2$ states the theory sketched in Sec. IV A assumes a particularly simple form because only a single nonzero quantum defect needs to be included. This reduces all matrix expressions to algebraic forms. Here we treat in detail the situation where two hydrogenic levels cross and are coupled by the core interaction. In particular, we retrieve from the density-of-states approach the simplified analysis sketched in Sec. III B and establish its validity. The algebraic details are given in the Appendix; only the results are summarized here. The starting point is the expression for the nonhydrogenic density of states, Eq. (4.2). For H^F and h^F we substitute two hydrogen parabolic channels with Lorentzian density of states, characterized by widths Γ_i and energy positions ϵ_i. The nonhydrogenic density of states D^F evaluated at the crossing exhibits the following behavior.

The density of states consists of two distinct Lorentzians if

$$4\,|\,\beta_{12}\,|^2 \gg \tfrac{1}{4}(\Gamma_1-\Gamma_2)^2 \; . \tag{4.5}$$

The positions and widths of the Lorentzians are the real and imaginary parts of the eigenvalues of the non-Hermitian energy matrix equation (3.1), where the absolute value of the interaction matrix element is identified with

$$|\,\beta_{12}\,|^2 = \tan^2\!\delta_l (U^0_{ln_1})^2 (U^0_{ln'_1})^2 \frac{d\epsilon}{d\Delta_1}\frac{d\epsilon}{d\Delta_2}\bigg|_{\epsilon_0} , \tag{4.6}$$

where $\pi d\epsilon/d\Delta$ is approximately the hydrogenic level spacing, $U^0_{ln_1}$ is a transformation matrix between spherical (here, $l=2$) and parabolic wave functions, and n_1,n'_1 are parabolic quantum numbers of the crossing hydrogenic states. This conclusion justifies the analysis of the $|\,M_L\,|=2$ measurement described in Sec. III B. At the anticrossing here are two nonoverlapping adiabatic states, each decaying exponentially in time [which was the key assumption in Eqs. (3.3) and (3.5)]. Because the initially stable state was populated at lower fields where it was very narrow ($< 10^{-20}$ cm^{-1}), its decay rate was determined solely by its ionization width rather than by the width of the excitation laser. Evaluation of Eq. (4.6) for the interaction matrix element gives $\beta_{12}=8.22\times10^{-9}$ a.u., which is in good agreement with the value derived from the simplified analysis based on Eq. (3.5) which approximately accounted for dynamic effects. Furthermore, it satisfies the inequality (4.5).

On the other hand, when the inequality (4.5) is not satisfied, application of an analysis based upon the non-Hermitian energy matrix equation (3.1) is no longer justified. In the limiting case of a very narrow state interacting with a very broad state with $|\,\beta\,|/\Gamma \ll 1$ (Γ is the width of the broad state), the density of states takes on a Beutler-Fano profile and the decay rate of the narrow state is given by the Fermi golden rule.[36] In intermediate cases the decay of the initially stable state presumably would depend on the detailed time history of the system and would not, in general, be exponential. This interesting phenomenon is clearly a subject for further study.

V. CONCLUSION

Our investigations show that it is possible to explain and, now even to predict, the occurrence of rich structure in ionization curves of highly excited helium atoms near the classical "saddle-point" ionization threshold F_{SP} in terms of the helium density of states. At field strengths slightly lower than F_{SP}, our results for the energy positions of helium Stark states are in excellent agreement with those of the matrix-diagonalization treatment employing a (large) truncated basis of discrete spherical states. At fields higher than F_{SP}, when the helium levels are significantly broadened, the theory enables evaluation of the level widths and, thus, of the ionization rates.

Although many details still have to be worked out, the agreement between measured ionization behavior and calculated ionization rates is good. The details especially concern the time dependence of the wave function in situations where narrow and broad states interact.

Since the core interaction needs only to be parametrized

by quantum defects, the field ionization of other atoms described by single-channel quantum-defect theory[37] can, in principle, be analyzed in a manner similar to that presented here for helium. In particular, the theory could readily be applied to evaluate the influence of the fine-structure interaction in the hydrogen atom on the ionization of hydrogen Stark states.[10]

Part of the field-ionization process is the dynamic response of highly excited atoms to time-varying fields, and it can enter in rather subtle, unexpected ways. A simplified analysis of this problem was used in the present paper, but a more detailed treatment awaits a forthcoming publication.

APPENDIX

Our purpose is to establish a relation between the eigenvalue of the non-Hermitian matrix equation (3.1) and the helium density of states.

Throughout this appendix we shall assume that there is only a single nonzero quantum defect $\mu=\delta/\pi$, in which case the scalar equations (4.2) and (4.3) can be used. The more general case of several nonzero quantum defects is treated by Harmin.[20] Where appropriate, we shall merely list the results of that treatment.

In the case of isolated hydrogenic resonances, H^F has a Lorentzian spectral line shape,

$$H^F = \alpha \frac{\Gamma/2}{(\epsilon-\epsilon_0)^2+(\Gamma/2)^2} , \tag{A1}$$

with

$$\alpha = (U^0_{ln_1})\frac{d\epsilon}{d\Delta}\bigg|_{\epsilon_0} ,$$

where $U^0_{ln_1}$ is a coefficient expressing the frame transformation between spherical (l) and parabolic (n_1) channels, and Δ is the phase accrued in the η potential well. Both are slowly varying functions of energy and are evaluated at the resonance center ϵ_0; $\pi d\epsilon/d\Delta$ is approximately the energy spacing of hydrogenic resonances. The dispersive companion of H^F is

$$h^F = \alpha \frac{\epsilon_0-\epsilon}{(\epsilon-\epsilon_0)^2+(\Gamma/2)^2} . \tag{A2}$$

Both expressions for H^F and h^F can equivalently be written as

$$H^F = \alpha\,\mathrm{Im}[(\epsilon-\epsilon_0-i\Gamma/2)^{-1}] ,$$

$$h^F = -\alpha\,\mathrm{Re}[(\epsilon-\epsilon_0-i\Gamma/2)^{-1}] . \tag{A3}$$

For convenience we repeat the analogous result for the nonhydrogenic density of states [Eq. (4.3)],

$$D^F = (\sin\delta)^{-2} \text{Im}[(\cot\delta - h^F - iH^F)^{-1}] \; . \tag{A4}$$

Substitution of Eq. (A3) into Eq. (A4) gives the density of states in the case of an isolated hydrogenic resonance perturbed by the influence of the core potential,

$$D^F = (\sin\delta)^{-2} \text{Im}\{[\cot\delta + \alpha/(\epsilon - \epsilon_0 + i\Gamma/2)]^{-1}\}$$

$$= \alpha(\cos\delta)^{-2} \frac{\Gamma/2}{(\epsilon - \epsilon_0 + \alpha\tan\delta)^2 + (\Gamma/2)^2} \; . \tag{A5}$$

It immediately follows that the spectral line shape of the nonhydrogenic resonance is also Lorentzian, its width is unchanged, and its center is shifted by $-\alpha\tan\delta$.

Alternatively, the shifted resonance center can be found from the zeros of the first term in the denominator of Eq. (4.2),

$$\cos\delta - \sin\delta \, h^F = 0 \; . \tag{A6}$$

One easily verifies that if $|\Gamma/\alpha\tan\delta| \ll 1$, one of the roots of Eq. (A6) gives the same resonance center as Eq. (A5). The other root is spurious because it lies very close to ϵ_0; the second term in the denominator of Eq. (4.2) is not small and it does not correspond to a maximum of D^F.

When two hydrogen Stark states labeled (1) and (2) below are coupled by the core potential, the resulting density of states follows in a similar fashion. The hydrogenic quantities H^F and h^F are now the sum of those for the individual states:

$$D^F = (\sin\delta\cos\delta)^{-1} \text{Im}\left[\left|1 + \frac{\alpha_1\tan\delta}{\epsilon - \epsilon_1 + i\Gamma_1/2} + \frac{\alpha_2\tan\delta}{\epsilon - \epsilon_2 + i\Gamma_2/2}\right|^{-1}\right]$$

$$= (\sin\delta\cos\delta)^{-1} \text{Im}\left[\frac{(\epsilon - \epsilon_1 + i\Gamma_1/2)(\epsilon - \epsilon_2 + i\Gamma_2/2)}{(\epsilon - \epsilon_1 + \alpha_1\tan\delta + i\Gamma_1/2)(\epsilon - \epsilon_2 + \alpha_2\tan\delta + i\Gamma_2/2) - \alpha_1\alpha_2\tan^2\delta}\right] \; . \tag{A7}$$

The zeros z_1 and z_2 of the denominator in the second part of Eq. (A7) coincide with the complex eigenvalues of the non-Hermitian matrix equation (3.1) if the interaction matrix elements are identified with $|\beta_{ij}|^2 = \alpha_i\alpha_j\tan^2\delta$. The core interaction prevents the hydrogenic levels from crossing. The position of the avoided crossing, defined as the minimum separation between the real part of the roots z_1 and z_2, is given by

$$\epsilon_1 - \alpha_1\tan\delta = \epsilon_2 - \alpha_2\tan\delta \; .$$

Expressed in terms of parameters of the hydrogen Stark structure and the helium quantum defect, the level separation at the anticrossing is $2\tan\delta(\alpha_1\alpha_2)^{1/2}$. When

$$\rho_L \equiv \frac{\frac{1}{2}|\Gamma_1 - \Gamma_2|}{2|\beta_{12}|} \ll 1 \; , \tag{A8}$$

Eq. (A7) may be written at the anticrossing as

$$D^F = (\cos\delta)^{-2} \text{Im}\left[\frac{\xi_1}{\epsilon - z_1} + \frac{\xi_2}{\epsilon - z_2}\right] \; , \tag{A9}$$

with

$$\xi_{1,2} = (\alpha_1 + \alpha_2)/2 \pm (\alpha_1\alpha_2)^{1/2} \; .$$

In this case the nonhydrogenic density of states is the sum of two Lorentzian line shapes. Their centers are the real parts of the respective eigenvalues of the non-Hermitian matrix equation (3.1), whereas their widths are the imaginary parts. At the anticrossing, therefore, are two distinct adiabatic states, each of which decays exponentially in time. This justifies the analysis presented in Sec. III B,

which explicitly assumed this time-dependent behavior of the wave function.

If the hydrogenic structure constants $\alpha_{1,2}$ are approximately equal, the intensity of one of the levels almost vanishes at the anticrossing. This has been experimentally observed by Zimmerman et al.[26] The results for the two-level anticrossing presented here are identical to those derived by Harmin,[20] who used a phase-matrix approach. However, the emergence of the parameter ρ_L, involving the difference of widths, is novel.

When $\rho_L \lesssim 1$, it can be shown that D^F reduces to the sum of two Beutler-Fano line shapes with a large asymmetry parameter $q = 2/\rho_L$. In the case of $\rho_L \simeq 1$ a more complicated interference pattern emerges, and the system will evolve in time in a more complicated fashion than a simple exponential decay.

When many hydrogenic resonances contribute to H^F and h^F, it is no longer possible to derive explicit expressions for the nonhydrogenic resonance positions and widths. In the case of several nonzero quantum defects the positions follow from

$$\det(\underline{Q}) = 0 \; , \tag{A10}$$

whereas the widths are given by

$$\left|\frac{d\epsilon}{d\det(\underline{Q})} \text{Tr}[(\text{cof}\underline{Q})\underline{H}^F \sin\underline{\delta}]\right| \; . \tag{A11}$$

Expression (A11) is evaluated at the zeros of the left-hand side of Eq. (A10) and the cofactor matrix is defined as $\text{cof}\underline{Q} = \underline{\tilde{Q}}^{-1}\det(\underline{Q})$.

*Present address: Philips Research Laboratories, 5600-JA Eindhoven, The Netherlands.

†Present address: Schlumberger-Doll Research, Ridgefield, CT 06877.

‡Present address: Physics Department, State University of New York at Stony Brook, Stony Brook, NY 11794-3800.

[1]J. R. Hiskes, C. B. Tarter, and D. A. Moody, Phys. Rev. **133**, A424 (1964); K. Omidvar, At. Data Nucl. Data Tables **28**, 215 (1983). To our knowledge, a theoretical treatment of simultaneous field-ionization decay and spontaneous radiative decay, when both rates are comparable, has not been carried out yet. However, for a step in this direction, see T. Bergeman, Phys. Rev. Lett. **52**, 1684 (1984).

[2]P. M. Koch and D. R. Mariani, Phys. Rev. Lett. **46**, 1275 (1981).

[3]R. J. Damburg and V. V. Kolosov, J. Phys. B **12**, 2637 (1979), and references therein, and in *Rydberg States of Atoms and Molecules*, Ref. 5. This latter reference contains the theoretical results that were compared in Ref. 2 to experimental results.

[4]P. M. Koch, in *Atomic Physics*, edited by D. Kleppner and F. M. Pipkin (Plenum, New York, 1981), Vol. 7.

[5]*Rydberg States of Atoms and Molecules*, edited by R. F. Stebbings and F. B. Dunning (Cambridge University Press, New York, 1983).

[6]H. J. Silverstone, B. G. Adams, J. Cizek, and P. Otto, Phys. Rev. Lett. **43**, 1498 (1979), and references therein.

[7]E. Luc-Koenig and A. Bachelier, J. Phys. B **13**, 743 (1980); **13**, 1769 (1980); Phys. Rev. Lett. **43**, 921 (1979).

[8]D. A. Harmin, Phys. Rev. A **24**, 2491 (1981).

[9]A useful review of the state of knowledge in this area up to the recent past may be found in D. Kleppner, M. G. Littman, and M. L. Zimmerman, in *Rydberg States of Atoms and Molecules*, Ref. 5, pp. 73—116.

[10]T. Bergeman, Ref. 1.

[11]T. S. Luk, L. Dimauro, T. Bergeman, and H. Metcalf. Phys. Rev. Lett. **47**, 83 (1981), and references therein.

[12]D. A. Harmin, Phys. Rev. A **26**, 2656 (1982).

[13]Compare R. F. Stebbings, C. J. Latimer, W. P. West, F. B. Dunning, and T. B. Cooke, Phys. Rev. A **12**, 1453 (1975); T. W. Ducas, M. G. Littman, R. R. Freeman, and D. Kleppner, Phys. Rev. Lett. **35**, 366 (1975); T. F. Gallagher, L. M. Humphrey, W. E. Cooke, R. M. Hill, and S. A. Edelstein, Phys. Rev. A **16**, 1098 (1977). Equation (1.1) can also be written in terms of an effective principal quantum number $n^* = n - \mu$, where μ is the quantum defect of the state. The saddle-point threshold field is then approximated by $F_{SP} = 1/16(n^*)^4$.

[14]M. B. Kadomtsev and B. Smirnov, Zh. Eksp. Teor. Fiz. **80**, 1715 (1981) [Sov. Phys.—JETP **53**, 885 (1981)].

[15]M. G. Littman, M. L. Zimmerman, and D. Kleppner, Phys. Rev. Lett. **37**, 486 (1976).

[16]M. G. Littman, M. M. Kash, and D. Kleppner, Phys. Rev. Lett. **41**, 103 (1978).

[17]T. H. Jeys, G. B. McMillian, K. A. Smith, F. B. Dunning, and R. F. Stebbings, Phys. Rev. A **26**, 335 (1982), and references therein.

[18]D. R. Mariani, W. van de Water, P. M. Koch, and T. Bergeman, Phys. Rev. Lett. **50**, 1261 (1983), considered the effect of many closely spaced anticrossings in helium that were traversed rapidly by exposure to a microwave electric field.

[19]J. R. Rubbmark, M. M. Kash, M. G. Littman, and D. Kleppner, Phys. Rev. A **23**, 3107 (1981). A single, isolated anticrossing was investigated in Na.

[20]D. A. Harmin, following paper [Phys. Rev. A **30**, 2413 (1984)].

[21]P. M. Koch, in *Rydberg States of Atoms and Molecules*, Ref. 5, pp. 473—512.

[22]Each of the two independent cw $^{12}C^{16}O_2$ lasers had an output power density of 5—20 W/cm². The technique used to stabilize the frequency of each laser to ~1 MHz ($\Delta v/v \simeq 3 \times 10^{-8}$) is described in W. H. Thomason and D. C. Elbers, Rev. Sci. Instrum. **46**, 409 (1975). The frequencies of the *P*- and *R*-branch transitions in the 9- and 10-μm bands are listed in C. Freed, L. C. Bradley, and R. G. O'Donnell, IEEE, J. Quant. Electron. **QE-16**, 1195 (1980). Corrections for those frequencies due to pressure and plasma effects in the lasing medium are given by H. W. Mocker [Appl. Phys. Lett. **12**, 20 (1968)], but they were negligible for the level of accuracy of our experiments.

[23]This condition is satisfied for states at the top of the $n=9$ manifold. Their Stark shift at a field strength of 200 V/cm is $O(1 \text{ cm}^{-1})$, whereas the fine-structure splitting is $< 10^{-2}$ cm^{-1}.

[24]The field plates F_3, F_4, and F_5 were constructed of two identical, planar subassemblies, each of which contained one side of the three electrode pairs. To fabricate a given subassembly, the insulating side of 0.16-cm-thick Cu-coated, G-10 fiberglass printed circuit board was bonded with epoxy to a 1.9-cm-thick aluminum support plate that was milled flat to about 10^{-3} cm. Because the circuit board was measured to have a thickness variation of $(2-3) \times 10^{-3}$ cm over the dimensions of the subassembly, the flatness of the backing plate could be transferred reasonably well to the Cu surfaces of the bonded circuit board. By chemically removing stripes of copper on the conducting side of the circuit board, the different plates in a given plane were electrrically isolated from each other. Opposing planar subassemblies were separated by precisely ground glass spheres and clamped together with screws. They were empirically tightened to optimize the measured parallelism of opposing planes. To minimize observed copper oxide surface-charging effects, the copper was gold-plated. These fabrication techniques are described in more detail in P. M. Koch, D. R. Mariani, and W. van de Water (unpublished). The field plates F_1 were made of stainless steel; they were stress-relieved in vacuum to remove spots with permanent magnetization induced by machining. The earth's and stray magnetic fields, whose components normal to the beam velocity could produce (motional) electric fields in the rest frame of the atoms, were reduced with use of Helmholtz coils and magnetic shielding. The latter was concentrated around the F_3-F_5 region, where fields were reduced below 15 mG. Thus, motional electric fields were reduced to less than 10 mV/cm. The field plates F_2 were made of aluminum sheet metal.

[25]P. M. Koch and D. R. Mariani, J. Phys. B **13**, L645 (1980); P. M. Koch, Ref. 21.

[26]M. L. Zimmerman, M. G. Littman, M. M. Kash, and D. Kleppner, Phys. Rev. A **20**, 2251 (1979).

[27]M. J. Seaton, Proc. Phys. Soc. London **88**, 815 (1966).

[28]D. R. Bates and A. Damgaard, Philos. Trans. R. Soc. London **242**, 101 (1949).

[29]This Stark spectrum used a slightly different excitation scheme from that of Fig. 2, namely

"7^3P" $(M_L = 0) \rightarrow$ "$9^3(L = 8)$" $(M_L = 0)$

$\rightarrow$ "$n = 18^3L$" $(M_L = 0)$.

The 9-μm *P*(16) laser line was used for the first (F_1) transi-

tion and its polarization was parallel to the field direction in F_1. The field strength was set at 25.78 kV/cm, whereas this transition was calculated to occur at 25.81 kV/cm. This 0.1% discrepancy should be compared to the 0.2% width of the Stark-tuned resonance peak and the ~0.3% uncertainty of the absolute determination of F_1, indicating good agreement. The laser interacting in F_3 was tuned to the 9-μm $P(14)$ line and polarized parallel to the field direction.

[30]G. B. McMillian, T. H. Jeys, K. A. Smith, F. B. Dunning, and R. F. Stebbings, J. Phys. B **15**, 2131 (1982).

[31]S. Feneuille, S. Liberman, E. Luc-Koenig, J. Pinard, and A. Taleb, J. Phys. B **15**, 1205 (1982), and private communication.

[32]W. E. Lamb, Jr., Phys. Rev. **85**, 259 (1952).

[33]E. Weber, *Electromagnetic Theory* (Dover, New York, 1965).

[34]D. R. Bates, Proc. R. Soc. London, Ser. A **257**, 22 (1960).

[35]There is an obvious and useful analogy here to the description of a collision between heavy particles in terms of (molecular) potential curves which approach each other at some internuclear separation. In the case in which the asymptotic field between the plates is set exactly at the crossing field, the variation of the energies with time in the fringe field is identical to the behavior of the potential curves in the Demkov model; see Yu. N. Demkov, Zh. Eksp. Teor. Fiz. **45**, 195 (1963) [Sov. Phys.—JETP **18**, 138 (1964)].

[36]L. Fonda, G. C. Ghirardi, and A. Rimini, Rep. Prog. Phys. **41**, 587 (1978).

[37]M. J. Seaton, Rep. Prog. Phys. **46**, 167 (1983).

[38]U. Fano, Phys. Rev. **124**, 1866 (1961).